RESEARCH

Enso influence on water vapor transport and thermodynamics over Northwestern South America

Melissa Ruiz-Vásquez[1,2] · Paola A. Arias[1,3] · J. Alejandro Martínez[1]

Abstract

The interannual variability of hydroclimatic conditions in Northwestern South America, especially precipitation, is mainly influenced by the El Niño–Southern Oscillation (ENSO). We explore potential mechanisms that affect precipitation occurrence in Northwestern South America during El Niño and La Niña events over the period 1980–2019, using data from the ERA5 reanalysis. We look at the atmospheric moisture contribution from different sources using the Dynamic Recycling Model to track water vapor trajectories. Interestingly, conditions with reduced precipitation during El Niño events can take place along with increased precipitable water. To understand this, we analyze thermodynamic conditions in the atmosphere that are necessary for precipitation to occur over the region, such as convective available potential energy, convective inhibition, lifting condensation level, and low-level relative humidity. With this approach, we find more favorable thermodynamic conditions for the occurrence of precipitation during La Niña events, even if the content of water vapor is equal or even less than during El Niño events. We also look at the structure of the regional Hadley and Walker circulation in both types of events and find that a weaker ascending motion during El Niño events also inhibits convection. This study provides an integral picture of how precipitation anomalies over Northwestern South America during ENSO events are related to dynamic and thermodynamic conditions and sources of atmospheric moisture.

1 Introduction

El Niño–Southern Oscillation (ENSO) is the main source of interannual hydroclimatic variability in Northwestern South America (NWSA), a region that is commonly referred as Northern South America (Poveda et al. 2006; Córdoba-Machado et al. 2015; Shimizu et al. 2017; Cai et al. 2020; Arias et al. 2021). The positive phase of ENSO, known as El Niño (EN), is associated with reduction in precipitation and increase in near-surface temperature over the region. By con-trast, its negative phase, known as La Niña (LN), is associated with an increase in precipitation and a reduction in near-surface temperatures (Poveda and Mesa 1996; Wang 2004; Capotondi et al. 2015; Salas et al. 2020). These changes in near-surface temperature associated with the ENSO phases modify the strength of the regional winds (both easterlies and westerlies) that also explain precipitation differences in both EN and LN due to reduced (increased) orographic low-level convergence during EN (LN) (Mesa-Sánchez and Rojo-Hernández 2020). Despite the tremendous efforts in studying this phenomenon, the mechanisms behind its effects at a regional and local scale in NWSA are still being under-stood (Canchala et al. 2020; Yan et al. 2020; Bolaños et al. 2021; Cerón et al. 2021; Sori et al. 2021).

Several studies have addressed the effects of ENSO in precipitation through the changes in atmospheric moisture contribution during both EN and LN events (Ropelewski and Halpert 1989; Castillo et al. 2014; Llamedo et al. 2017; Sulca et al. 2018; Sori et al. 2021). Particularly for NWSA, Arias et al. (2015) indicate that the anomalous wet season during the period 2010–2012 was mainly controlled by an enhanced moisture contribution from the Caribbean sea, the tropical Atlantic ocean, and the eastern Pacific ocean. From another perspective, Hoyos et al. (2019b) evaluate the spatio-

✉ Melissa Ruiz-Vásquez
  mruiz@bgc-jena.mpg.de

  Paola A. Arias
  paola.arias@udea.edu.co

  J. Alejandro Martínez
  john.martinez@udea.edu.co

[1] Escuela Ambiental, Universidad de Antioquia, Calle 67 No. 53–108, Medellín, Antioquia, Colombia

[2] Biogeochemical Integration, Max Planck Institute for Biogeochemistry, Hans-Knöll-Straße 10, Jena 07745, Germany

[3] Grupo de Ingeniería y Gestión Ambiental (GIGA), Universidad de Antioquia, Medellín, Colombia

temporal variability of atmospheric moisture in NWSA on seasonal and interannual time scales and emphasize the role of the Intertropical Convergence Zone-induced circulation and the low-level jets as the most important sources for this variability. As a final example, Morales et al. (2021) highlight the role of the low-level jets in moisture transport, for instance, in different ENSO regimes. They show that during LN, the low-level circulation jet over western Colombia, known as the Choco Jet (Poveda and Mesa 1999, 2000), strengthens the wind shear over the region, a key mechanism in atmospheric moisture advection. These previous studies suggest that increases in precipitation in NWSA, during strong LN events for example, are characterized by an enhanced moisture transport of surrounding regions which is also associated with changes in regional circulation.

In comparison to the effects on atmospheric moisture contribution, less attention has been given to ENSO effects on thermodynamics over NWSA. Nevertheless, there are some studies that show the strong effect of thermodynamics on precipitation patterns over specific regions. Lintner and Boos (2019) explore the relationship between the South Pacific Convergence Zone and ENSO events through a 2D approach of atmospheric energy transport. They show that water and energy flux anomalies during ENSO dominate the South Pacific Convergence Zone shift. Bayr et al. (2021) quantify the thermodynamic feedbacks between the ocean and the atmosphere through sea surface temperatures and heat fluxes simulated by climate models. They suggest that the better the representation of thermodynamic feedbacks between the ocean and the atmosphere, the more realistic is the simulation of ENSO events. This highlights the importance of thermodynamic processes as the main drivers in the response of precipitation to ENSO events.

A supporting mechanism of these thermodynamic drivers is the Hadley cell (Ye et al. 1998). Riemann-Campe et al. (2009) present a global climatology of the thermodynamic indices convective available potential energy (CAPE) and convective inhibition (CIN). They show that large values of CAPE may be associated with conditions in the ascending branch of the Hadley circulation, while large values of CIN would be characteristically seen for conditions in the descending branch. The Hadley cell also plays a role in the response of precipitation during ENSO events (Guo and Li 2016). Kayano et al. (2019) study the regional circulation patterns in terms of the Walker and Hadley cells during LN events. They find that variations in both cells affect precipitation in South America during LN events due to an enhancement of the rising motions. By contrast, for the EN events, the weakened rising motion and the strengthened downward motion of the Hadley cell play the key roles. However, Rollings and Merlis (2021) find that the relationship between ENSO and the Hadley cell is strong only when considering low-frequency variability in the ENSO signal.

In light of the importance of (i) atmospheric moisture advection, (ii) thermodynamic feedbacks, and (iii) regional circulation patterns in response to ENSO events, we analyze the effects of EN and LN in precipitation over NWSA and the main drivers underlying the ENSO precipitation response. First, we quantify the atmospheric moisture contribution from different sources to NWSA (and the contribution of NWSA to itself, i.e., atmospheric moisture recycling). Second, we analyze various thermodynamic parameters related to atmospheric instability and that are usually associated with the occurrence of precipitation. Third, we look at the response of the regional Hadley cell in terms of the rising and sinking motions of air parcels.

2 Data and methods

2.1 Study area

We perform our analyses on the regional domain of tropical South America, shown in Fig. 1. To study the atmospheric water vapor transport, we divide this domain in different subregions (sinks and sources of atmospheric moisture), following the approaches of Arias et al. (2015), Agudelo et al. (2019), and Ruiz-Vásquez et al. (2020) of big continental basins. These subregions are based on the Pfafstetter delineation of basins, level 1 (Verdin and Verdin 1999), and latitudinal classification of oceanic sources. We focus in the NWSA subregion as a sink of atmospheric moisture during EN and LN phases.

NWSA is an interesting region in terms of hydroclimatic variability arising from its equatorial setting and its neighboring Caribbean sea and tropical Pacific ocean. Moreover, it displays large topographic gradients due to the three branches of the Andes crossing from southwest to the northeast, which
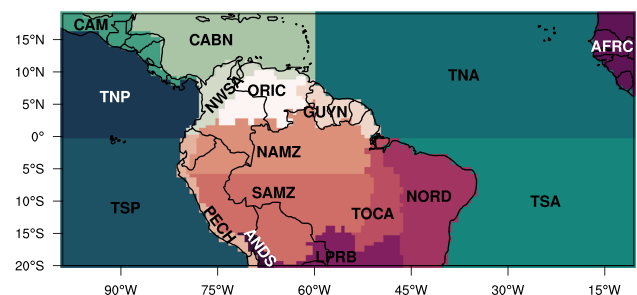

Fig. 1 Domain considered to estimate water vapor transport towards Northwestern South America (NWSA) using the DRM. TNP, Tropical North Pacific; TSP, Tropical South Pacific; TNA, Tropical North Atlantic; TSA, Tropical South Atlantic; CAM, Central America; CABN, Caribbean Sea; ORIC, Orinoco basin; GUYN, Guyanas; PECH, Peru-Chile; NAMZ, Northern Amazon; SAMZ, Southern Amazon; TOCA, Tocantins basin; NORD, Brazilian Nordeste; LPRB, La Plata River Basin; AFRC, Africa; ANDS, Subtropical Andes

propitiates strong land-atmosphere feedbacks (Poveda et al. 2011). The boundaries for this region follow the coastlines and the topography of the eastern branch of the Andes.

Arias et al. (2015) quantify the total water vapor contribution to NWSA from the considered sources. They account for approximately 79% of the total atmospheric moisture that reaches NWSA. The remaining 21% may be due to moisture imbalances depicted by the input atmospheric fields and additional losses in the numerical schemes of the Dynamic Recycling Model (DRM). The fundamentals of the DRM are further explained in Section 2.3.

2.2 ENSO events

To select the periods corresponding to each ENSO phase (EN and LN), we examine the Oceanic Niño Index (ONI) (NOAA 2023; Glantz and Ramirez 2020). This index considers the 3-month running mean of sea surface temperature anomalies of the tropical Pacific ocean averaged over the region 5° N–5° S, 170° W–120 °W. Although the ONI can be calculated for any period, in this study, we calculate the ONI over the period 1980–2019 which is a suitable length to compute climatology values and is the available data period (see Section 2.3) at the moment of computations. For a season to be considered as part of an ENSO event, the ONI values must exceed ±0.5 °C for at least five consecutive months. This is the operational definition used by the National Oceanic and Atmospheric Administration (NOAA). We show in Table 3 the classification of seasons as EN (red) and LN (blue) events during the period 1980–2019.

We focus our analyses only on the differences in atmospheric and thermodynamic-related variables between EN and LN events that are statistically significant according to a Bootstrap test (Efron 1992). For this purpose, we generate 1000 data samples with replacement. We consider only significant differences according to a significance threshold of 95% (Agudelo et al. 2019). We choose Boostraping since it does not make any *a priori* assumption about the distribution of the sample data.

2.3 Atmospheric moisture sources

We use the DRM to track the atmospheric humidity from different source to sink regions during ENSO events. NWSA is the sink region of interest in this study. The DRM is a 2D analytical model that uses a semi-Lagrangian approach to estimate the spatio-temporal variation of the atmospheric moisture that is recycled in a target region (i.e., that originates as evapotranspiration in the same region) and is advected to and from other remote regions (Dominguez et al. 2006; Martínez and Dominguez 2014; Ruiz-Vásquez et al. 2020). The model is derived from the water vapor conservation equation integrated into the atmosphere and can be used for time scales from days (because it does not assume that any change in the storage term of the conservation equation is negligible) to monthly and larger scales. The mathematical formulation of the DRM is discussed by Dominguez et al. (2006).

Further, Martínez and Dominguez (2014) develop a method to identify the contributions from each source region to a given sink region. It allows decomposing the trajectory of the plot when it reaches the sink region to identify in which regions the humidity of each part of the trajectory was generated. This method also allows quantifying the contribution of the same target region to its own humidity (i.e., moisture recycled).

Despite treating the atmosphere as a single layer, Roy et al. (2019) and Morales et al. (2021) find that the DRM performs well in regions with complex topography. Both studies find differences between the vertical integration of the fluxes and the low-level winds in terms of magnitude. Nevertheless, the variability (in terms of anomalies and correlations) is the same in both cases. Therefore, the DRM may be effectively used to study atmospheric transport changes in the context of different ENSO phases.

We analyze the climatological interannual variability of water vapor transport in NWSA associated to EN and LN events. We use atmospheric sub-daily data from the ERA5 reanalysis (Hersbach et al. 2020), at a resolution of 0.5° for the period 1980–2019 (see Table 1) in the domain covered

Table 1 Variables obtained from the ERA5 reanalysis to be used in the DRM

Variable	Time (hour)
Evaporation	00:00, 12:00
Total precipitation	00:00, 12:00
Vertically integrated water vapor from the Earth's surface to the top of the atmosphere	00:00, 06:00, 12:00, 18:00
Vertical integral of eastward water vapor from the Earth's surface to the top of the atmosphere	00:00, 06:00, 12:00, 18:00
Vertical integral of northward water vapor from the Earth's surface to the top of the atmosphere	00:00, 06:00, 12:00, 18:00

by latitudes 20° S–19° N and longitudes 99° W–10.5° W, as shown in Fig. 1.

2.4 Thermodynamic indices

In addition to the atmospheric moisture transport estimates, we analyze thermodynamic indices related to precipitation occurrence. Particularly, we consider the following variables from the ERA5 reanalysis, in accordance to Chen et al. (2017):

- **Convective available potential energy (CAPE):** it is an indicator of the instability (or stability) of the atmosphere. This index assesses the potential for the development of convection, which can lead to precipitation, but it is not the only condition for precipitation to occur. Large positive values of CAPE indicate that an air parcel would be much warmer than its surrounding environment, very buoyant, suggesting great potential for severe weather (Gizaw et al. 2021).
- **Convective inhibition (CIN):** in counterpart to CAPE, CIN is a measure of the amount of energy required for convection to occur. High values of this parameter indicate that deep and moist convection is unlikely to occur even if CAPE is large. Therefore, these two indices are complementary (Gizaw et al. 2021).
- **Lifting condensation level (LCL):** it is the height in the atmosphere at which the Relative Humidity (RH) of an air parcel reaches 100% when it is cooled by dry adiabatic lifting from the surface. It is an estimation of the convective cloud-base height (Shi et al. 2021). In general, high cloud bases over the tropics indicate hot dry land surfaces.
- **Low-level relative humidity (RH):** humidity at low levels is important for convective initiation (Todd et al. 2018). Here, we use data of low-level RH as an average over the 1000–850 hPa layer.

For these variables, we consider monthly averages at two different hours a day: 06 UTC and 18 UTC, which represent nighttime (01:00 LT) and daytime (13:00 LT) over NWSA, respectively. We choose these two-time slices to represent two extremes in the diurnal cycle of precipitation in NWSA, as described in Bedoya-Soto et al. (2019). During midnight, the mature phase of the mesoscale convective systems is mainly formed. At noon, NWSA experiences the time of maximum heating and therefore has most of the potential to produce rainfall. Rainfall events in NWSA can be observed during both time slices.

In addition to the previously listed thermodynamic indices, we also analyzed: total precipitable water vapor, relative humidity in the middle troposphere (700–400 hPa), shal-

low vertical wind shear (vector wind difference between 3 and 1 Km), and deep vertical wind shear (vector wind difference between 1 and 9 Km). Nevertheless, we decided not to include these in the current study since they did not show to be significantly different between EN and LN events.

2.5 Regional Hadley and Walker cells

Finally, we consider the response of the regional Hadley and Walker cells in tropical South America to ENSO events. For the regional Hadley cell, we follow the approach formulated by Zhang and Wang (2013) to calculate a regional mass-stream function (Ψ) without violating the principle of negligible net transport of zonal mass. This approach uses the meridional component of the irrotational flow, which contributes to the vertical motion in the north-south circulation represented by the Hadley cell. We calculate the meridional mass-stream function of the regional Hadley circulation over tropical South America, as shown by the Eq. 1.

$$\Psi = \frac{2\pi \cos(\phi)}{g} \int_0^p [v_{IR}] dP \tag{1}$$

where ϕ is the latitude and v_{IR} is the irrotational component of the meridional wind averaged for longitudes 70° W–50° W. Similar to the thermodynamic indices described in Section 2.4, we obtain the monthly wind fields to compute the irrotational component of the meridional wind from the ERA5 reanalysis at 06 UTC and at 18 UTC.

For the regional Walker cell, we use the zonal component of the irrotational flow that contributes to vertical motion in the East-West circulation and it is computed for the 99° W–10.5° W longitudinal band. The irrotational component of the zonal wind is averaged over 0°–10° N, to assess the changes in the Walker circulation over NWSA.

3 Results

3.1 Atmospheric moisture contributions to NWSA during ENSO events

Figure 2 shows the annual cycle of precipitable water and the annual cycle of the terms of the moisture balance (precipitation, evaporation, and residual term) that are contributed from all the sources included in Fig. 1 to NWSA during EN and LN events. From February to July, we see more precipitable water contributed during EN (PWEN) with respect to the precipitable water contributed during LN (PWLN), whereas the contribution from August to January is approximately equal in both EN and LN events. However, this contribution does not correspond to the respective contribution in precipitation.

Fig. 2 Annual cycle of total **a** precipitable water, **b** precipitation, **c** evaporation, and **d** residual term of the moisture balance averaged over NWSA during EN (red) and LN (blue) events. C, P, and E in panel **d** denote Convergence, Precipitation, and Evaporation, respectively. Note that precipitable water has units of mm because this is a storage variable, as opposite to the other variables that have units of mm d^{-1} because these are flux variables
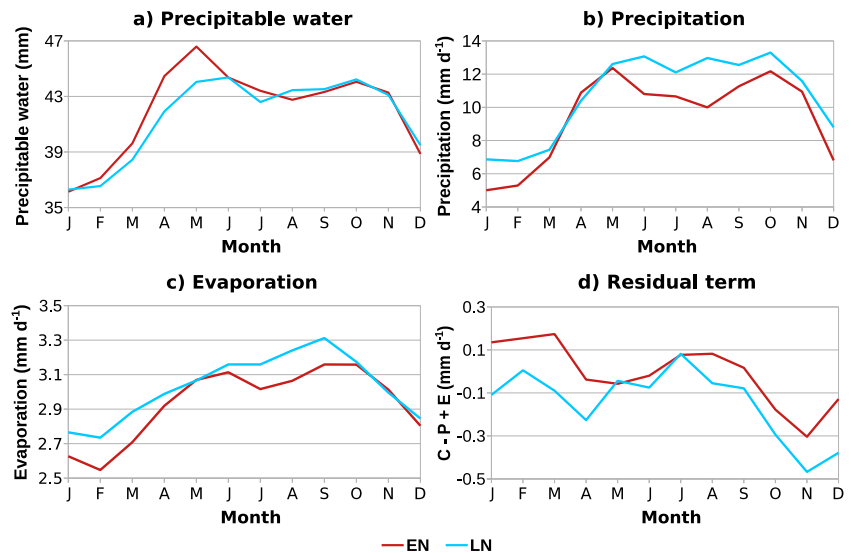

In general, we see a higher contribution in precipitation to NWSA during LN than during EN events. The annual cycle of the evaporation term (Fig. 2c) shows more contribution to the atmosphere during LN than during EN, especially in the months with higher precipitation values (January–March and June–September). Similar to precipitation, the annual cycle of convergence shows higher contribution to the water balance during LN with regards to EN (see Appendix A Fig. 14).

The net income of moisture to each atmospheric column can be represented by the residual term (TR) as shown by Eq. 2.

$$TR = C + E - P = \frac{d(PW)}{dt} - RES_w \qquad (2)$$

where C, P, and E denote convergence, precipitation, and evaporation, respectively. RES_w represents the residual forc-

Fig. 3 PWEN–PWLN contribution to NWSA (brown line) during the DJF season from the sources **a** TNA, **b** TNP, **c** CABN, **d** ORIC, **e** NWSA, **f** GUYN, and **g** NAMZ. Reddish (blueish) colors represent reduction (increment) of PWEN with respect to PWLN. White background represents no significant differences according to a Bootstrap test. Vectors represent the difference in VIMF
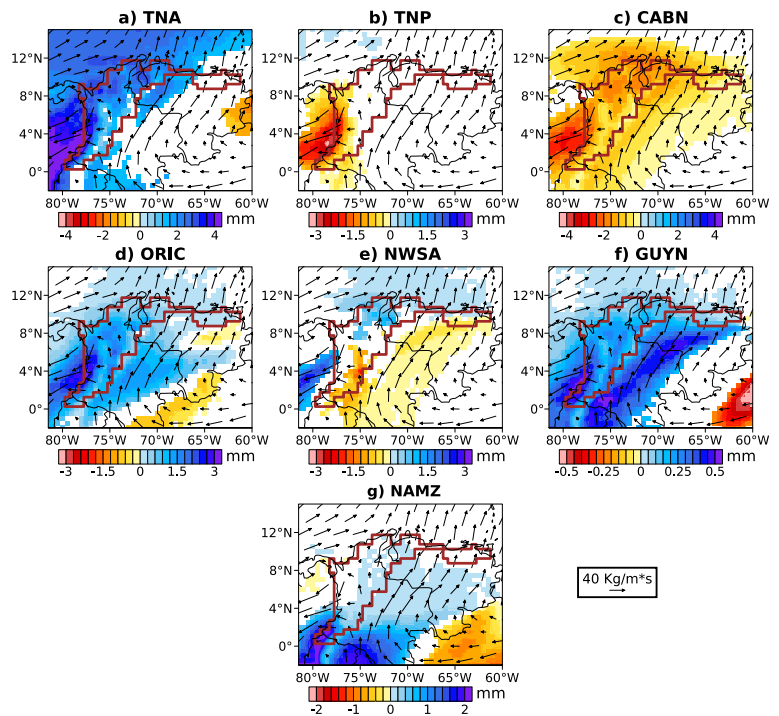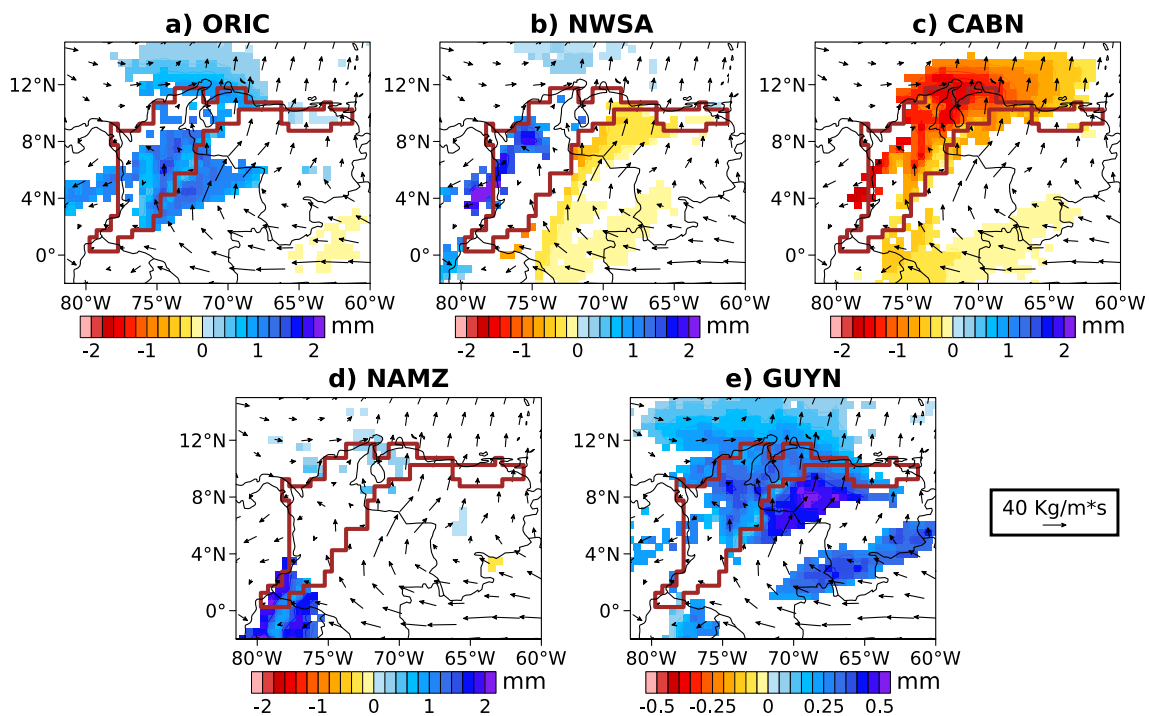
Fig. 4 PWEN–PWLN contribution to NWSA (brown line) during the MAM season from the sources **a** ORIC, **b** NWSA, **c** CABN, **d** NAMZ, and **d** GUYN. Reddish (blueish) colors represent the reduction (increasing) of PWEN with respect to PWLN. White background represents no significant differences according to a Bootstrap test. Vectors represent the difference in VIMF

ing associated with the analysis increments in the reanalysis, and $\frac{d(PW)}{dt}$ is the rate of change in the water vapor content in an atmospheric column, which at intra-annual time scales can be nonnegligible (Lorenz and Kunstmann 2012). Since the intra-annual behavior of atmospheric variables is important for the different ENSO phases; here, we include TR averages for each month of the year for composites of EN and LN years (Fig. 2d).

In general, the TR term is much smaller in magnitude than the other terms in the atmospheric water balance Eq. (2). However, TR is larger during EN than during LN, particularly during the first half of the year (Fig. 2d), which may be related with a sharper increase in PW between February and May during EN years (Fig. 2a). In other words, the net income of moisture as estimated by TR (i.e., subtracting the output due to precipitation from the inputs associated with moisture convergence and surface evaporation) is larger during EN, leaving a moister atmosphere during the first part of the year, even during months when precipitation is nearly the same in EN and LN years (Fig. 2b).

Between May and September, the TR term is rather similar between EN and LN, with values closer to 0, associated with similar values of PW in both phases of ENSO, with smaller changes during this time of the year. Between October and December, the TR is negative, associated with similar rates

of decrease in PW during the last part of the year, starting from similar PW values in October for both phases of ENSO. The negative values of TR during periods with increasing PW could be related with the error-like term RES_w. For example, Rodell et al. (2015) found that the error in the closure of the atmospheric water budget equation for South America is negative, with an average value of -0.07mm/day.

We quantify the changes in atmospheric moisture advection and recycling within the regions considered during both EN and LN events. Figures 3, 4, 5, and 6 show PWEN–PWLN (colors) and the differences in vertically integrated moisture fluxes (VIMF; vectors) for each season: December–February (DJF), March–May (MAM), June–August (JJA) and September–November (SON), respectively. The climatological EN and the differences between EN and LN composites for VIMF are shown in the Appendix A Fig. 15. Figure 3 reveals that there is more contribution of PWEN to NWSA from Tropical North Atlantic (TNA), Orinoco (ORIC), Guyanas (GUYN), and northern Amazon (NAMZ) than PWLN. Similar results were found by Kim et al. (2019). Also, there is less contribution of PWEN from Caribbean (CABN) and Tropical North Pacific (TNP) than PWLN. Regarding the moisture recycling (Fig. 3e), we see a dipole in the NWSA atmospheric moisture contribution to itself, which coincides with a weakening of the VIMF vectors in
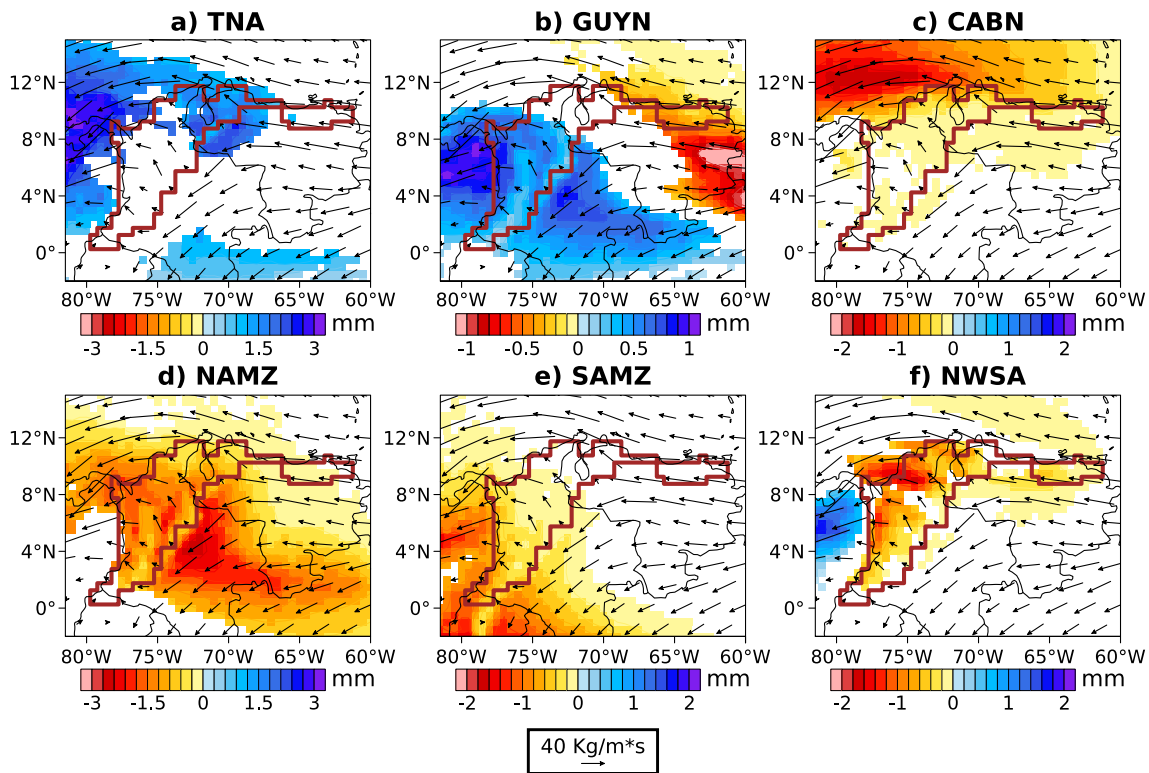
Fig. 5 PWEN–PWLN contribution to NWSA (brown line) during the JJA season from the sources **a** TNA, **b** GUYN, **c** CABN, **d** NAMZ, **e** SAMZ, and **f** NWSA. Reddish (blueish) colors represent reduction (increment) of PWEN with respect to PWLN. White background represents no significant differences according to a Bootstrap test. Vectors represent the difference in VIMF

the northern part of NWSA during EN with respect to LN that sequentially suppresses southward moisture transport during EN.

For MAM, Fig. 4 shows in general more number of source regions (ORIC, NWSA, NAMZ, and GUYN) with an increase in their contribution of PWEN to NWSA with respect to PWLN than source regions with a decrease in their contribution, which coincides with Fig. 2. Only CABN contributes less during EN than during LN events. During this season, we do not see a substantial difference in VIMF vectors over the NWSA subregion.

During JJA, we see significant changes in moisture contribution from the regions shown in Fig. 5. TNA and GUYN are the only sources that contribute more PWEN to NWSA than PWLN. CABN, NAMZ, and Southern Amazon (SAMZ) contribute less PWEN. The moisture recycling in NWSA is also less during EN. VIMF vectors over Central America (CAM) are strengthened in EN during this season in relation to LN, and this factor endorses the westward atmospheric moisture advection. These positive and negative contributions are of similar magnitude and thus they compensate, leaving a similar amount of atmospheric moisture over NWSA, as observed in Fig. 2.

Finally, for SON, we mostly see less contributions of PWEN to NWSA from the considered regions (Fig. 6) with respect to PWLN. Only TNA contributes more moisture during EN than during LN. This is also linked to a weaker low-level jet over western Colombia, known as the Choco Jet, as discussed by Gallego et al. (2019). Similar to what happens during JJA (Fig. 5), VIMF vectors over CAM are strengthened during EN, favoring the atmospheric moisture advection towards more western regions.

The moisture transport shown in Figs. 3, 4, 5, and 6 must be considered along with atmospheric moisture flux convergence (See Appendix A Fig. 15). All year round, there is less convergence over NWSA during EN than during LN. In terms of the moisture contribution to NWSA, the low convergence values during EN, with regards to LN, explain the low precipitation values seen, which suggests that larger values of monthly mean precipitable water (Fig. 2a) are available during EN at the same time when the fluxes associated with moisture convergence (see Appendix A Fig. 14 and precipitation (Fig. 2b) are reduced.

The percentage change in precipitable water contribution to NWSA from the sources considered in Figs. 3, 4, 5, and 6 during LN relative to EN events is shown in Table 2. The most noteworthy changes are from TNP, GUYN, and SAMZ, but these sources only contribute to NWSA approximately in 6% of the total atmospheric moisture, and therefore changes in these sources are small in absolute terms. Changes from TNA
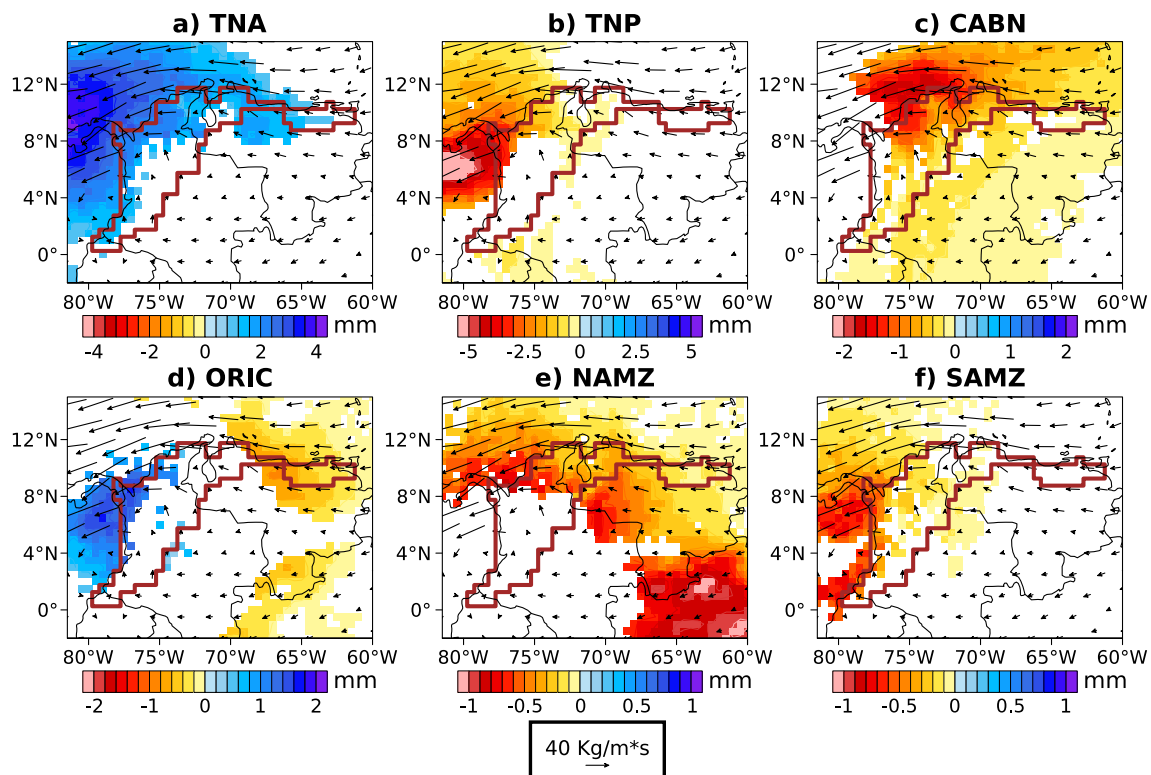
Fig. 6 PWEN–PWLN contribution to NWSA (brown line) during the SON season from the sources **a** TNA, **b** TNP, **c** CABN, **d** ORIC, **e** NAMZ, and **f** SAMZ. Reddish (blueish) colors represent reduction (increment) of PWEN with respect to PWLN. White background represents no significant differences according to a Bootstrap test. Vectors represent the difference in VIMF

and NWSA are more meaningful because these sources contribute in approximately 45% of the total moisture in NWSA. Changes in CABN, ORIC, and NAMZ are also important because they contribute in 19% to the total moisture over NWSA (Arias et al. 2015). MAM is the season with the most remarkable change in precipitable water, as seen also in Fig. 2a.

Table 2 Percentage change (%) of atmospheric moisture contribution of each source to NWSA during LN with respect to the contribution of the same source during EN

	DJF	MAM	JJA	SON
TNP	224.37	122.22	326.17	153.27
TNA	88.74	99.98	90.17	89.37
CABN	147.18	159.08	138.78	137.76
NWSA	102.22	94.76	118.07	101.08
ORIC	68.27	81.29	99.22	90.41
GUYN	40.81	72.32	82.52	91.88
NAMZ	69.42	72.11	130.57	112.47
SAMZ	434.39	146.79	437.85	198.48
Total	100.16	95.28	99.93	100.16

Blue(red) indicates increased (decreased) contribution

3.2 Thermodynamic indices during ENSO events

Now, we aim to understand the counter-intuitive response of precipitation to the available precipitable water during the ENSO phases. What does happen with the extra humidity from February to June in the atmosphere during EN in relation to LN? Why does it not precipitate? Which mechanisms favor the precipitation during LN from May to March? We try to solve these questions from a thermodynamic perspective, quantifying the values of the indices described in Section 2.4 and the regional Hadley and Walker cells, as introduced in Section 2.5.

We look at some thermodynamic conditions (indices) necessary for precipitation to occur, as described in Section 2.4. We focus only on their values over NWSA during local nighttime (06 UTC) and local daytime (18 UTC), which correspond to time slices with high occurrence of precipitation over this region (Bedoya-Soto et al. 2019).

Large values of CAPE are often associated with precipitation since convection takes place. Figure 7 shows the differences in CAPE composites between EN and LN events. In general, CAPE is higher over NWSA during EN than during LN events for all seasons, specially at nighttime. This
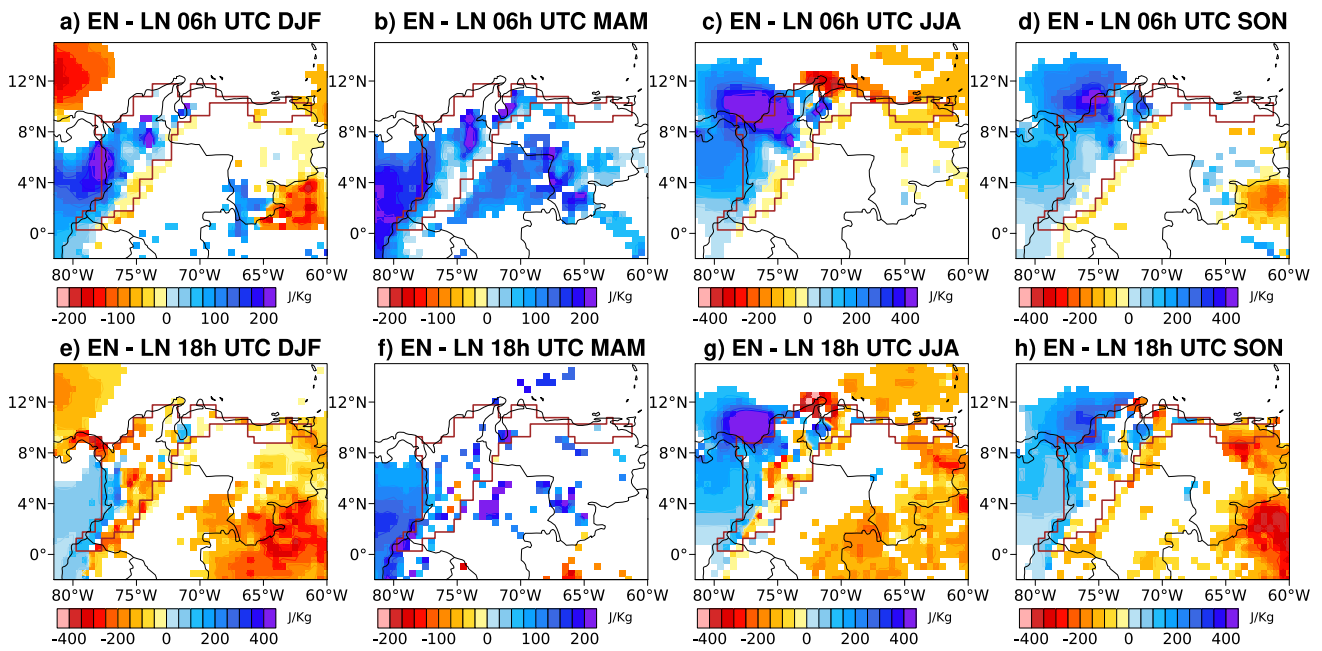
Fig. 7 Seasonal differences in CAPE between EN and LN events at **a–d** 06 h UTC and **e–h** 18 h UTC

index suggests that precipitation would more likely occur during EN, which is not what we observe from the response of precipitation in Fig. 2b. However, it is necessary to consider other indices in order to evaluate the occurrence of precipitation. Furthermore, given the complex topography of NWSA and the observed diurnal cycle, precipitation maximum is equally likely to occur during the afternoon and midnight (Poveda et al. 2005).

However, in many situations CAPE cannot be released unless CIN has a small value (Markowski and Richardson 2010). High values of CIN represent the amount of energy that is still required for the development of convective systems and therefore suggest the non-occurrence of precipitation. In Fig. 8, we see high positive values of CIN across NWSA during all the seasons, especially at daytime (18 UTC) for the EN–LN composites. This pattern agrees
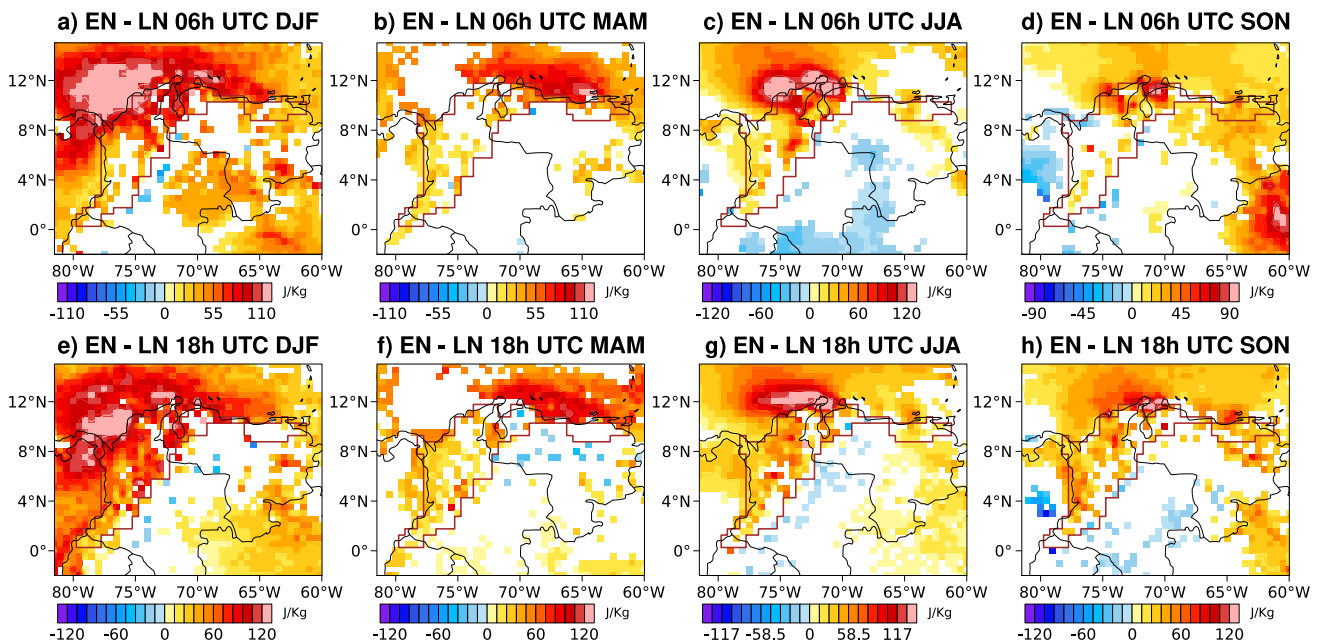

Fig. 8 Seasonal differences in CIN between EN and LN events at **a–d** 06 h UTC and **e–h** 18 h UTC
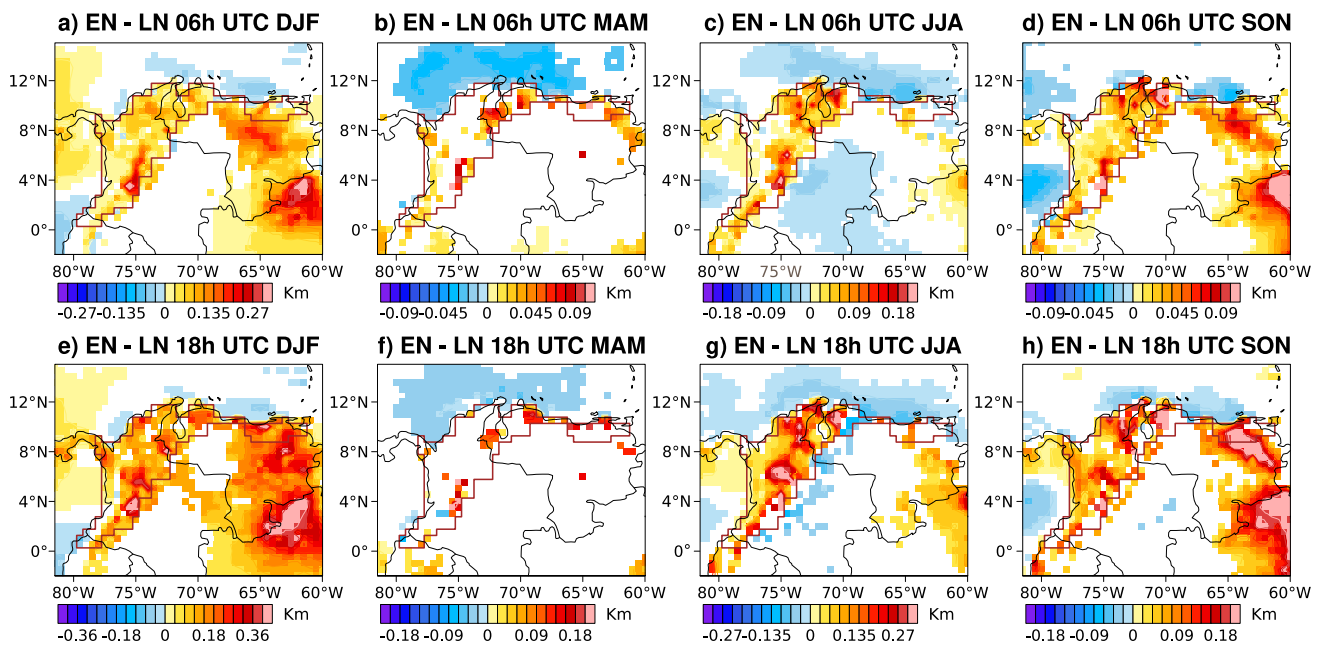
Fig. 9 Seasonal differences in LCL between EN and LN events at **a–d** 06 h UTC and **e–h** 18 h UTC

with: *(i)* the non-occurrence of precipitation for EN events during the first semester of the year, in which there is more atmospheric humidity, and *(ii)* the favoring of precipitation during the second semester of the year, in which humidity over NWSA is more similar in both EN and LN events, as observed in Fig. 2a.

A third thermodynamic index considered is the LCL. High values of this index in tropical regions indicate high altitude

of cloud-base which suggests hot and dry surface conditions. Figure 9 shows that the cloud-base during EN events is higher than during LN events. MAM was the only season that did not show significant differences for this index between the two ENSO phases, but also it is the season when there are small differences in terms of precipitation between both EN and LN events (Fig. 2b). The greatest differences in LCL are found
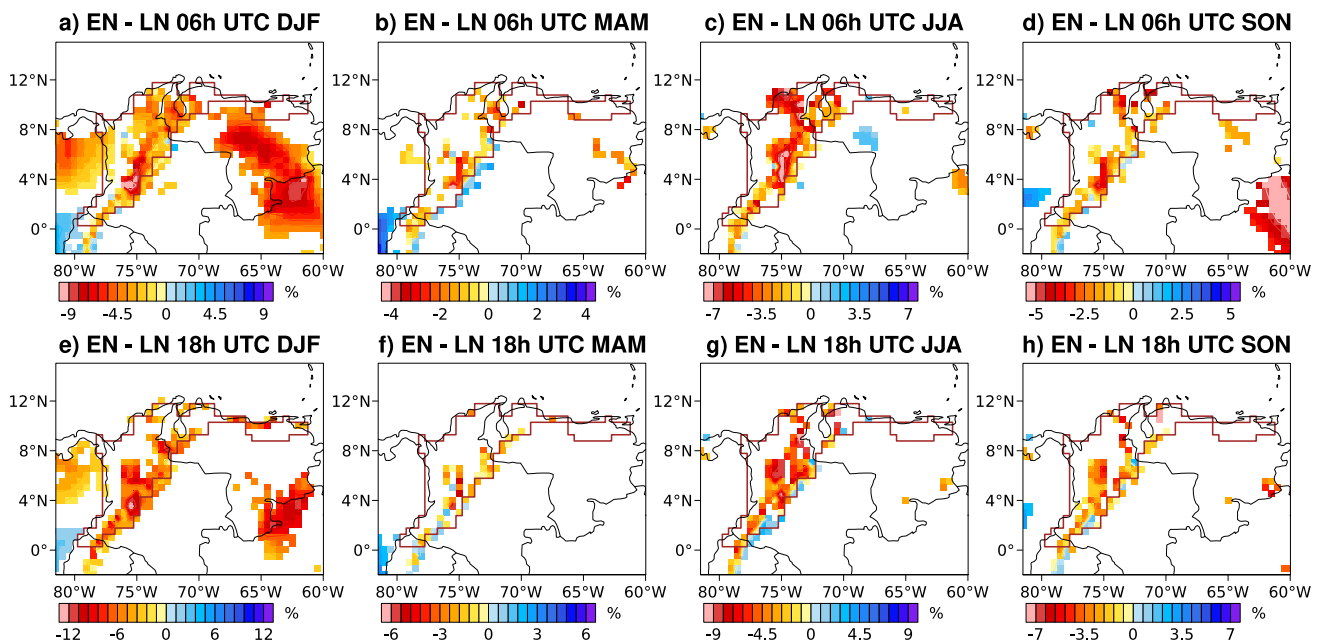

Fig. 10 Seasonal differences in low-level RH between EN and LN events at **a–d** 06 h UTC and **e–h** 18 h UTC

during DJF and JJA when the differences in precipitation are also the greatest.

The final thermodynamic index analyzed is the low-level RH (the RH contained in the atmospheric layer between 1000 and 850 hPa; Fig. 10). This index is particularly important during DJF, with less RH during EN than during LN. Even though there is more atmospheric humidity available in this season during EN events (Fig. 2a), the atmosphere is warmer and therefore the RH can be lower, inhibiting the occurrence of condensation and precipitation. In particular, variations of RH during ENSO have been investigated by Todd et al. (2018), who find a strong correlation between RH

and precipitation shifts during ENSO events, highlighting the importance of this variable as a predictor of precipitation shifts in modeled ENSO events.

3.3 Regional Hadley and Walker cells during ENSO events

To support the findings discussed in Section 3.2, we also look at the response of the regional Hadley and Walker circulation over NWSA to the ENSO phases. Figures 11 and 12 show the mean vertical motion at latitudes and longitudes that cover the NWSA subregion. The ascending branch of the Hadley

Fig. 11 Vertical cross-sections of the regional mass-stream function (contours) averaged over 70° W–50° W during **a** DJF, **b** MAM, **c** JJA, and **d** SON for EN events (first column) and the difference between EN and LN events (second column). Vectors represent the divergent component of the meridional wind (in m/s) and the vertical negative pressure velocity (in 10^3 hPa/s)
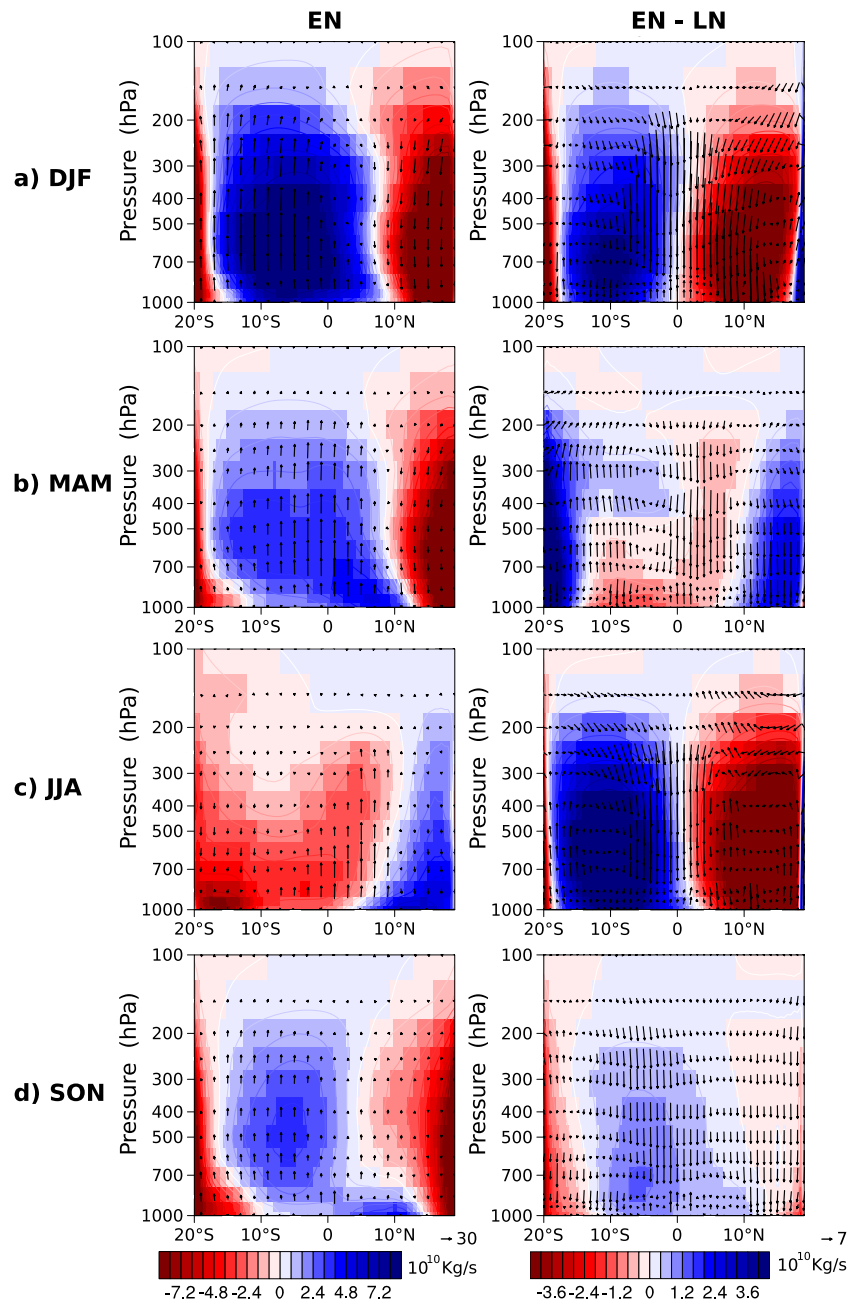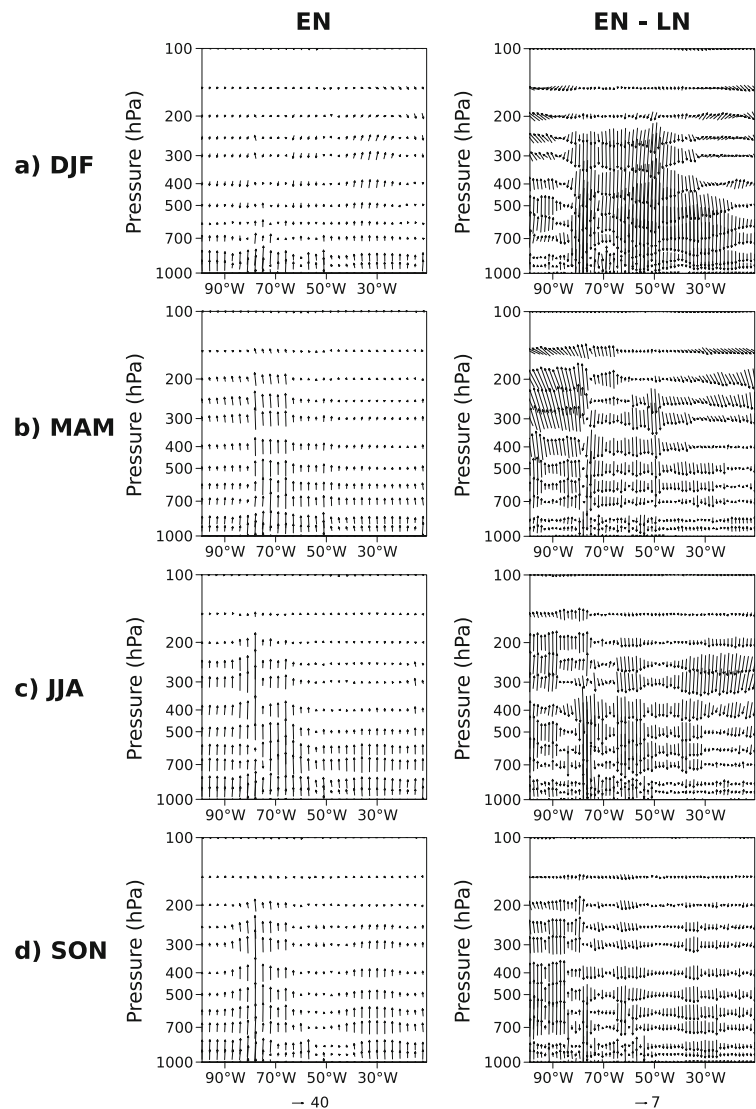
Fig. 12 Divergent component of the zonal wind (in m/s) and the vertical negative pressure velocity (in 10^3 hPa/s) averaged over 0° N–10° N during **a** DJF, **b** MAM, **c** JJA, and **d** SON for EN events (first column) and the difference between EN and LN events (second column)

cell is located over the latitudes of the Summer Hemisphere. Similarly, the ascending branch of the Walker cell is favored from MAM until SON, and it is stronger during JJA, around 70°W.

The ascending motions favor the development of convective systems and therefore the occurrence of precipitation, whereas the descending motions inhibit precipitation. In the first and third rows of Fig. 11, we can see how this ascending branch shifts from one to another side of the Equator between seasons, being around 10°S during DJF (Austral Summer) and around 8°N during JJA (Boreal Summer). During the transition seasons (MAM and SON), the ascending branch is not clear and spans over more latitudes. The second and fourth rows in Fig. 11 show the differences in this vertical motion between EN and LN events. In terms of the Walker cell (Fig. 12), we see a weakening of the ascending motion during all seasons in EN events, specially over the NWSA

subregion (around 75°W). In most cases, the weakening of the ascending motion over NWSA is stronger in lower levels of the troposphere, but during JJA the weakening is also strong in the middle levels.

Overall, we see a weakening in the ascending motions during EN events and a strengthening in the descending motions during LN events, favoring the inhibition of precipitation during EN, as first discussed by Kousky et al. (1984) and Ropelewski and Halpert (1987). This weakening (strengthening) of the ascending (descending) motion during EN is also consistent with the results from Martín-Gómez et al. (2020) and Sátori et al. (2009). The weakening (strengthening) of the ascending (descending) motion is particularly strong during DJF and JJA. Thus even though there is slightly more precipitable water in the atmosphere for both seasons during EN (Fig. 2a), the ascending motion is inhibited and so the development of convective systems and precipitation during

EN events (Fig. 2b). The strengthened response in precipitation during LN shows that the also strengthened ascending motion in this phase compensates a lower available humidity (Fig. 2a).

Finally, for the rainy seasons in NWSA (MAM and SON), we see that the weakening of the ascending motion during EN is associated with the difference in precipitation with respect to LN. For MAM, we see the largest differences in precipitable water over NWSA between both ENSO phases (precipitable water being greater during EN), but the increased ascending motion during LN makes precipitation values very similar to that of EN. For SON, even though the amount of precipitable water is very similar in both phases, precipitation is strengthened during LN (Fig. 2b) due to an enhanced ascending motion.

4 Discussion and conclusions

The aim for this study is to investigate the following question: what are the atmospheric conditions, in terms of regional circulation, atmospheric moisture transport, and thermodynamics, over Northwestern South America (NWSA) during the phases of El Niño–Southern Oscilation (ENSO)? We find that during about half of an El Niño (EN) year, there is more precipitable water than during a La Niña (LN) year, despite the fact that precipitation can be greater during the latter. Besides the change in the atmospheric moisture sources, we also explore the role of plausible dynamic and thermodynamic mechanisms for such changes. Our findings are summarized in Fig. 13.

Using the Dynamic Recycling Model (DRM), we compute the trajectories of water vapor transport over the region. The quantified amount of precipitable water in water vapor tracking models is highly sensitive to the residence time of water vapor in the atmosphere considered by the models (Gimeno et al. 2021; Nieto and Gimeno 2019), which could lead to over/underestimations in the atmospheric moisture contribution. However, the DRM performance has been shown to be adequate for NWSA in comparison to other more complex 3D models like FLEXPART (Hoyos et al. 2018; Morales et al. 2021), especially when studying atmospheric changes in moisture transport under different regimes, as we do here.

From February to July, we see more contribution from the different sources during EN than during LN events, although the contribution is similar between both phases for the remaining months. The contributions from the Atlantic
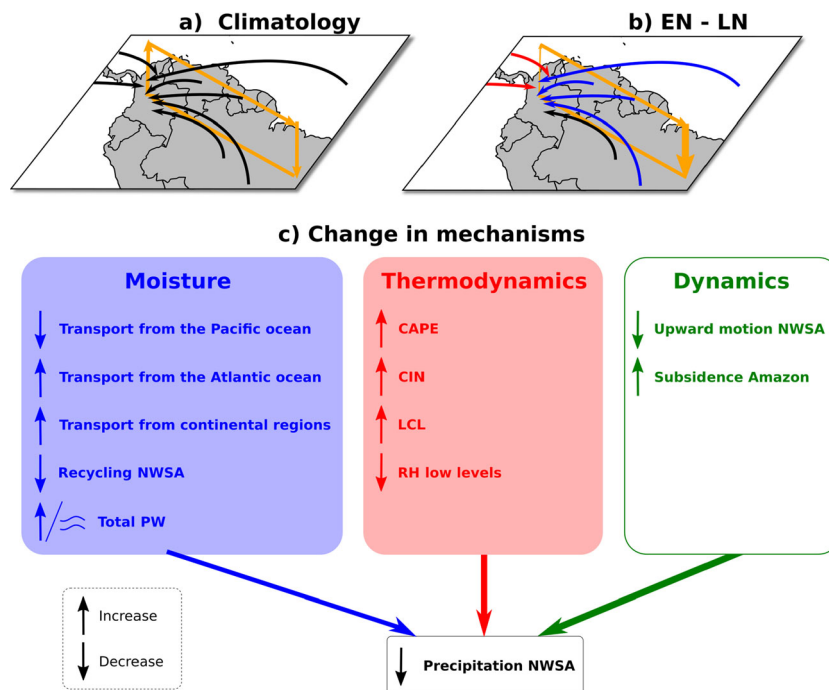

Fig. 13 Schematic illustrating key changes in atmospheric moisture transport, thermodynamic indices, and regional circulation across North Western South America (NWSA) during ENSO events. **a** Represents the climatology of the atmospheric moisture transport from various sources to NWSA (black arrows) and the regional Hadley cell (yellow arrows). **b** Represents the differences between EN and LN phases, where red (blue) arrows denote reduced (increased) atmospheric moisture transport while black arrows denote negligible changes. **c** Provides a summary of significant changes in different mechanisms: atmospheric moisture transport (blue solid rectangle), thermodynamic indices (red solid rectangle), and regional dynamics (green transparent rectangle) over NWSA, where solid (transparent) background color indicates novel (previously known) insights into the mechanisms influencing precipitation in NWSA during ENSO phases

ocean and continental subregions increase, whereas the contributions from the Pacific ocean and the moisture recycling in NWSA decrease (Fig. 13). The response of precipitation to these changes during ENSO is nonlinear. The amount of precipitation largely depends on the available precipitable water (Chen et al. 2017), but also on local conditions such as atmospheric stability, advection rate, and regional circulation patterns. We find that precipitable water is larger during EN compared to LN during the first part of the year, despite having nearly the same or even more precipitation during LN years. In this part of the year, there is a higher net income of moisture due to convergence and evaporation during EN, which along with less precipitation is leaving a moister atmosphere, compared with LN conditions. In this sense, precipitation during the first part of the year would be controlled by additional factors, e.g., thermodynamics, but not by the availability of moisture alone. In other words, thermodynamic and/or dynamic factors may drive precipitation during the first part of the year, which in turn impacts the amount of precipitable water remaining in the atmosphere.

Accordingly, we look at the response of some thermodynamic indices and the atmospheric regional circulation over NWSA to both ENSO phases. These aspects strongly influence the occurrence of precipitation, as suggested by Chen et al. (2017) and Liu et al. (2020). To account for the thermodynamics, we consider four indices: convective available potential energy (CAPE), convective inhibition (CIN), lifting condensation level (LCL), and low-level relative humidity (RH). The changes identified in the last three indices agree with the already observed changes of precipitation over NWSA during the ENSO phases.

From a thermodynamic perspective, precipitation is less favored during EN events because *(i)* there is more energy required for convection to occur (higher CIN), *(ii)* the air parcels reach saturation at higher altitudes (higher LCL), and *(iii)* the lowest levels in the atmosphere have less RH, which makes the condensation process more difficult. CAPE is also larger during EN years, but this is not surprising (despite the similar or reduced precipitation) since with less precipitation and anomalous subsidence conditions, we can have more solar radiation reaching the surface, more heating, higher near-surface temperature, thus increasing the potential temperature of air parcels, finally increasing CAPE (Dommenget 2010). However, this available energy cannot be released when CIN is relatively large, as in EN years.

The atmospheric general circulation over NWSA is induced by diabatic heating (Mesa-Sánchez and Rojo-Hernández 2020). In places where precipitation largely exceeds evaporation, such as typically in NWSA, a significant amount of latent heat becomes available to influence the atmospheric circulation. When there is another heating source nearby, for instance in front of the coasts of Perú during EN events, the westerly winds move further south. This results in a decrease of the magnitude of the westerly winds entering NWSA as we see in our results with the reduced moisture advection from the Pacific ocean. In response, the easterly winds increase and so the moisture advection from the Atlantic ocean and eastern continental sources increases as well.

As a last mechanism to explain precipitation occurrence during EN and LN, we study the response of the regional Hadley and Walker cells to these phases. Similar to what we find with the thermodynamic indices, the regional cells also support the favoring of precipitation during LN. We see a weaker (stronger) ascending motion during EN (LN) events over NWSA during all the seasons, which inhibits (enhances) the upward motion of air masses and condensation processes over the region. This result also reinforces the findings by Ropelewski and Halpert (1987), who highlight the subsidence over NWSA due to a westward displacement of the Walker circulation during EN.

According to the atmospheric water budget, the precipitation rate is related to changes in precipitable water, not just to its absolute value. Therefore, a large value of precipitable water could be associated with little precipitation provided that precipitable water does not change too much on a given interval of time (e.g., no increase with time). In this study larger values of precipitable water during EN years (compared to LN years, Fig. 2a) are found to be associated with a net increase in moisture from convergence and evaporation when precipitation is less or even nearly the same. In this sense, precipitation would be more controlled by other factors like thermodynamics (e.g., CIN) and the regional circulation (e.g., anomalous subsidence), with increased precipitable water as a consequence rather than driving factor. The extra precipitation observed during LN is associated with asymmetric changes in the regional circulation (Hadley cell) that intensify the atmospheric moisture convergence and favor unstable thermodynamic environments. Finally, these asymmetric changes in regional circulation are linked to an enhancement of atmospheric moisture transport from particular sources during LN with respect to EN, including those from the Pacific ocean. The Atlantic ocean and continental sources like ORIC and the Northern Amazon dominate during EN.

Thermodynamic conditions and the regional circulation play key roles in the response of precipitation over NWSA during EN and LN events, even more than the mere availability of atmospheric moisture, as seen for the first part of the year (Figs. 2 and 13). For example, during the 2015 flash flood event in La Liboriana basin in Salgar, Colombia (Hoyos et al. 2019a), the regional circulation and the atmospheric convection strengthened the orographically-enhanced heavy precipitation episode that triggered a flash flood, even under negative monthly precipitation anomalies during an EN year. There are other extreme cases in which the content of water

vapor can dominate the response of precipitation during LN events, as shown by Arias et al. (2015), who find that the anomalous wet season in NWSA during 2010–2012 was largely controlled by extra moisture contributions from the adjacent oceans. Nevertheless, this was a very unique LN event, in terms of its impacts in the region (Boening et al. 2012; Hoyos et al. 2013). In this study, we consider the average of all EN and LN events during the period 1980–2019, from which we can see that thermodynamics and regional circulation have a dominant role in the occurrence of precipitation. Changes in the atmosphere-ocean coupling due to ENSO variability modify air temperature over land and therefore the atmospheric stability, which is essential for precipitation to occur. Moreover, land-atmosphere interactions over NWSA are shown to be important during the ENSO phases (Bedoya-Soto et al. 2018, 2019; Cai et al. 2020)

Previous studies show that NWSA is particularly sensitive to the influence of ENSO (Poveda and Mesa 1996; Poveda et al. 2006; Hoyos et al. 2019b; Salas et al. 2020; Arias et al. 2021). In general, EN events induce reductions in precipitation and runoff in the region (Córdoba-Machado et al. 2015; Serna et al. 2018; Canchala et al. 2020) while LN events are associated with the opposite (Hoyos et al. 2013; Arias et al. 2015). Poveda et al. (2006) discuss some physical mechanisms associated with the influence of ENSO in NWSA. Among these aspects, they highlight that decreases in precipitation over NWSA during EN years are related to: *(i)* the reduction of atmospheric moisture transport inland from the eastern Pacific, in association with a weaker Choco jet; *(ii)* an anomalous Hadley cell with subdued ascent of moist air over NWSA; *(iii)* the displacement of the convective centers within the Intertropical Convergence Zone in the eastern equatorial Pacific towards the west and south of their climatological location; *(iv)* a weak feedback between precipitation and surface convergence associated with the Hadley circulation and the trade winds; and *(v)* the disruption of land-atmosphere interactions due to the regional coupling between anomalies of precipitation, soil moisture, vegetation, and evapotranspiration, with reduced evapotranspiration inducing a reduction of evaporation recycling.

Our results support that EN events are characterized by reduced atmospheric moisture transport from the Tropical North Pacific to NWSA, enhanced air subsidence over the region in association with anomalous regional Hadley and Walker cells, reduced moisture convergence in NWSA, and reduced atmospheric moisture recycling over the region. In addition, our work provides further evidence of the key role played by the regional atmospheric circulation and thermodynamics in the mechanisms for ENSO influence on precipitation in NWSA. In this sense, the reduced precipitation observed over NWSA during EN years with respect to LN is not a matter of reduced atmospheric moisture transport towards the region. In fact, EN years exhibit enhanced water vapor transport to NWSA from most of its main moisture sources with respect to LN, however this available atmospheric water does not precipitate. The inhibition of precipitation in NWSA during EN arises from a more stable atmosphere characterized by enhanced CIN, higher LCL, and reduced RH in the lower levels. The combination of a more stable atmosphere with an enhanced subsidence motion in NWSA due to an anomalous Hadley cell overcomes the increases of precipitable water in the region, inducing a reduction of precipitation during EN years in comparison with LN. This reveals the importance of considering not only the dynamic aspects and moisture sources for precipitation but also the thermodynamics involved, particularly in a region with very complex land-atmosphere interactions.

Appendix A

Table 3 Classification of seasons in El Niño (red) and La Niña (blue) events

DJF	MAM	JJA	SON
1982–1983	1982	1982	1982
1983–1984	1983	1985	1983
1984–1985	1985	1987	1984
1986–1987	1987	1988	1986
1987–1988	1989	1991	1987
1988–1989	1992	1997	1988
1991–1992	1998	1998	1991
1994–1995	1999	1999	1994
1995–1996	2000	2000	1995
1997–1998	2008	2002	1997
1998–1999	2011	2004	1998
1999–2000	2012	2007	1999
2000–2001	2015	2009	2000
2002–2003	2016	2010	2002
2004–2005	2018	2011	2004
2005–2006	2019	2015	2006
2006–2007			2007
2007–2008			2009
2008–2009			2010
2009–2010			2011
2010–2011			2014
2011–2012			2015
2014–2015			2016
2015–2016			2017
2017–2018			2018
2018–2019			
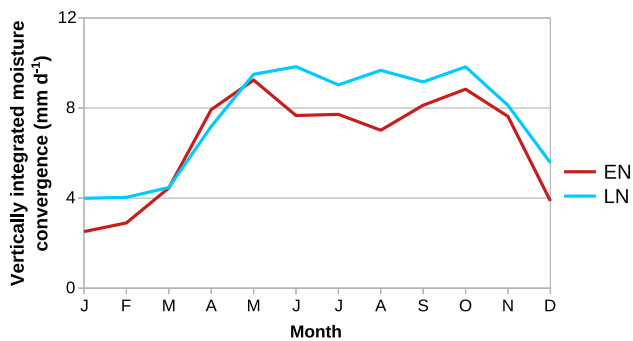
Fig. 14 Seasonal cycle of convergence over NWSA for EN (red) and LN (blue)

Fig. 15 Seasonal vertically integrated moisture flux (VIMF; vectors) for EN (left column) and the difference between EN and LN events (right column)
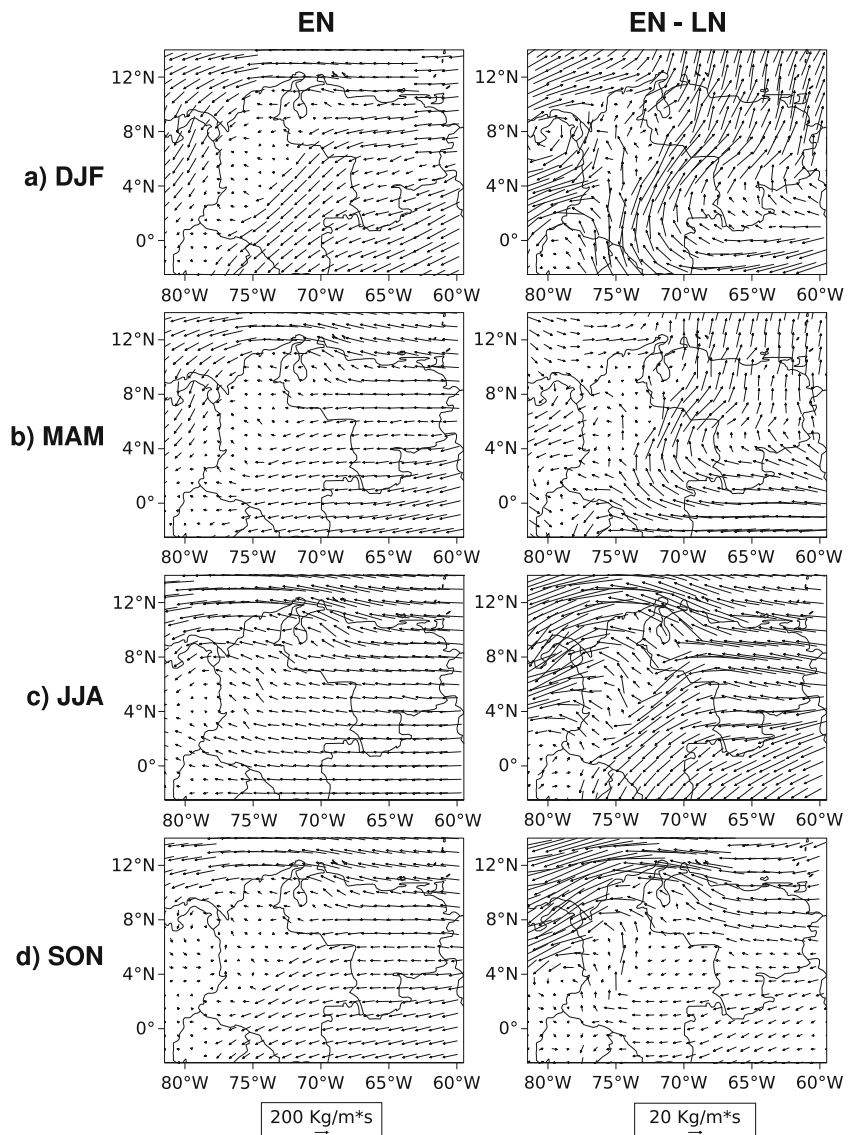
Declarations

Conflict of interest The authors declare no competing interests.

References

Agudelo J, Arias PA, Vieira SC et al (2019) Influence of longer dry seasons in the southern Amazon on patterns of water vapor transport over Northern South America and the Caribbean. Clim Dyn 52(5–6):2647–2665. https://doi.org/10.1007/s00382-018-4285-1

Arias PA, Martínez JA, Vieira SC (2015) Moisture sources to the 2010–2012 anomalous wet season in Northern South America. Clim Dyn 45(9–10):2861–2884. https://doi.org/10.1007/s00382-015-2511-7

Arias PA, Garreaud R, Poveda G et al (2021) Hydroclimate of the Andes part II: hydroclimate variability and sub-continental patterns. Front Earth Sci 8:666. https://doi.org/10.3389/feart.2020.505467

Bayr T, Drews A, Latif M et al (2021) The interplay of thermodynamics and ocean dynamics during ENSO growth phase. Clim Dyn 56(5). https://doi.org/10.1007/s00382-020-05552-4

Bedoya-Soto JM, Poveda G, Sauchyn D (2018) New insights on land surface–atmosphere feedbacks over tropical South America at interannual timescales. Water 10(8). https://doi.org/10.3390/w10081095

Bedoya-Soto JM, Aristizábal E, Carmona AM et al (2019) Seasonal shift of the diurnal cycle of rainfall over Medellin's Valley, Central Andes of Colombia (1998–2005). Front Earth Sci 7. https://doi.org/10.3389/feart.2019.00092

Boening C, Willis JK, Landerer FW et al (2012) The 2011 La Niña: so strong, the oceans fell. Geophys Res Lett 39(19). https://doi.org/10.1029/2012GL053055

Bolaños S, Salazar JF, Betancur T et al (2021) GRACE reveals depletion of water storage in Northwestern South America between ENSO extremes. J Hydrol 596(125):687. https://doi.org/10.1016/j.jhydrol.2020.125687

Cai W, McPhaden MJ, Grimm AM et al (2020) Climate impacts of the El Niño-Southern Oscillation on South America. Nat Rev Earth Environ 1:215–231. https://doi.org/10.1038/s43017-020-0040-3

Canchala T, Loaiza Cerón W, Francés F et al (2020) Streamflow variability in Colombian Pacific basins and their teleconnections with climate indices. Water 12(2). https://doi.org/10.3390/w12020526

Capotondi A, Wittenberg AT, Newman M et al (2015) Understanding ENSO diversity. Bull Am Meteorol Soc 96(6):921–938. https://doi.org/10.1175/BAMS-D-13-00117.1

Castillo R, Nieto R, Drumond A et al (2014) The role of the ENSO cycle in the modulation of moisture transport from major oceanic moisture sources. Water Resour Res 50(2):1046–1058. https://doi.org/10.1002/2013WR013900

Cerón WL, Kayano MT, Andreoli RV et al (2021) Rainfall variability in southwestern Colombia: changes in ENSO-related features. Pure Appl Geophys 178:1087–1103. https://doi.org/10.1007/s00024-021-02673-7

Chen B, Liu C, Mapes BE (2017) Relationships between large precipitating systems and atmospheric factors at a grid scale. J Atmos Sci 74(2):531–552. https://doi.org/10.1175/JAS-D-16-0049.1

Córdoba-Machado S, Palomino-Lemus R, Gámiz-Fortis SR et al (2015) Assessing the impact of El Niño Modoki on seasonal precipitation in Colombia. Glob Planet Chang 124:41–61. https://doi.org/10.1016/j.gloplacha.2014.11.003

Dominguez F, Kumar P, Liang XZ et al (2006) Impact of atmospheric moisture storage on precipitation recycling. J Clim 19(8):1513–1530. https://doi.org/10.1175/JCLI3691.1

Dommenget D (2010) The slab ocean El Niño. Geophys Res Lett 37(20). https://doi.org/10.1029/2010GL044888

Efron B (1992) Bootstrap methods: another look at the Jackknife, Springer New York, pp 569–593. https://doi.org/10.1214/aos/1176344552

Gallego D, García-Herrera R, Gómez-Delgado FDP et al (2019) Tracking the moisture transport from the Pacific towards Central and Northern South America since the late 19th century. Earth System Dynamics 10(2):319–331. https://doi.org/10.5194/esd-10-319-2019

Gimeno L, Eiras-Barca J, Durán-Quesada AM et al (2021) The residence time of water vapour in the atmosphere. Nat Rev Earth Environ 2:558–569. https://doi.org/10.1038/s43017-021-00181-9

Gizaw MS, Gan TY, Yang Y et al (2021) Changes to the 1979–2013 summer convective available potential energy (CAPE) and extreme precipitation over North America. Physics and Chemistry of the Earth, Parts A/B/C 123(103):047. https://doi.org/10.1016/j.pce.2021.103047

Glantz MH, Ramirez IJ (2020) Reviewing the Oceanic Niño Index (ONI) to enhance societal readiness for El Niños impacts. Int J Disaster Risk Sci 11:394–403. https://doi.org/10.1007/s13753-020-00275-w

Guo YP, Li JP (2016) Impact of ENSO events on the interannual variability of Hadley circulation extents in boreal winter. Adv Clim Chang Res 7(1–2):46–53. https://doi.org/10.1016/j.accre.2016.05.001

Hersbach H, Bell B, Berrisford P et al (2020) The ERA5 global reanalysis. Quarterly Journal of the Royal Meteorological Society 146(730):1999–2049. https://doi.org/10.1002/qj.3803

Hoyos N, Escobar J, Restrepo J et al (2013) Impact of the 2010–2011 La Niña phenomenon in Colombia, South America: the human toll of an extreme weather event. Appl Geogr 39:16–25. https://doi.org/10.1016/j.apgeog.2012.11.018

Hoyos I, Dominguez F, Cañón-Barriga J et al (2018) Moisture origin and transport processes in Colombia, Northern South America. Climate dynamics 50(3–4):971–990. https://doi.org/10.1007/s00382-017-3653-6

Hoyos CD, Ceballos LI, Prez-Carrasquilla JS, et al (2019) Meteorological conditions leading to the 2015 Salgar flash flood: lessons for vulnerable regions in tropical complex terrain. Nat Hazards and Earth Syst Sci 19(11):2635–2665. https://doi.org/10.5194/nhess-19-2635-2019

Hoyos I, Cañón-Barriga J, Arenas-Suárez T et al (2019) Variability of regional atmospheric moisture over Northern South America: patterns and underlying phenomena. Clim Dyn 52:893–911. https://doi.org/10.1007/s00382-018-4172-9

Kayano MT, Andreoli RV, Souza RAFd (2019) El Niño-Southern Oscillation related teleconnections over South America under distinct Atlantic Multidecadal Oscillation and Pacific Interdecadal Oscillation backgrounds: La Niña. Int J Climatol 39(3):1359–1372. https://doi.org/10.1002/joc.5886

Kim HM, Zhou Y, Alexander MA (2019) Changes in atmospheric rivers and moisture transport over the Northeast Pacific and Western North America in response to ENSO diversity. Clim Dyn 52(12):7375–7388. https://doi.org/10.1007/s00382-017-3598-9

Kousky VE, Kagano MT, Cavalcanti IFA (1984) A review of the Southern Oscillation: oceanic-atmospheric circulation changes and related rainfall anomalies. Tellus A 36A(5):490–504. https://doi.org/10.1111/j.1600-0870.1984.tb00264.x

Lintner BR, Boos WR (2019) Using atmospheric energy transport to quantitatively constrain South Pacific Convergence Zone shifts during ENSO. Journal of Climate 32(6):1839–1855. https://doi.org/10.1175/JCLI-D-18-0151.1

Liu N, Liu C, Chen B et al (2020) What are the favorable large-scale environments for the highest-flash-rate thunderstorms on earth? J Atmos Sci 77(5):1583–1612. https://doi.org/10.1175/JAS-D-19-0235.1

Llamedo P, Hierro R, de la Torre A et al (2017) ENSO-related moisture and temperature anomalies over South America derived from GPS radio occultation profiles. Int J Climatol 37(1):268–275. https://doi.org/10.1002/joc.4702

Lorenz C, Kunstmann H (2012) The hydrological cycle in three state-of-the-art reanalyses: intercomparison and performance analysis. J Hydrometeorol 13(5):1397–1420. https://doi.org/10.1175/JHM-D-11-088.1

Markowski P, Richardson Y (2010) Mesoscale meteorology in midlatitudes, vol 1. John Wiley & Sons. https://doi.org/10.1002/9780470682104

Martínez JA, Dominguez F (2014) Sources of atmospheric moisture for the La Plata river basin. J Clim 27(17):6737–6753. https://doi.org/10.1175/JCLI-D-14-00022.1

Martín-Gómez V, Barreiro M, Losada T et al (2020) Southern hemisphere circulation anomalies and impacts over subtropical South America due to different El Niño flavours. Int J Climatol 40(14):6201–6218. https://doi.org/10.1002/joc.6577

Mesa-Sánchez OJ, Rojo-Hernández JD (2020) On the general circulation of the atmosphere around Colombia. RACCEFYN 44(172):857-875. https://doi.org/10.18257/raccefyn.899

Morales JS, Arias PA, Martínez JA et al (2021) The role of low-level circulation on water vapour transport to Central and Northern South America: insights from a 2D Lagrangian approach. Int J Climatol 41(S1):E2662–E2682. https://doi.org/10.1002/joc.6873

Nieto R, Gimeno L (2019) A database of optimal integration times for Lagrangian studies of atmospheric moisture sources and sinks. Sci Data 6. https://doi.org/10.1038/s41597-019-0068-8

NOAA (2023) Cold and warm episodes by season. https://origin.cpc.ncep.noaa.gov/products/analysis_monitoring/ensostuff/ONI_v5.php, accessed: 2023-10-23

Poveda G, álvarez DM, Rueda óA (2011) Hydro-climatic variability over the Andes of Colombia associated with ENSO: a review of climatic processes and their impact on one of the earth's most important biodiversity hotspots. Clim Dyn 36(11):2233–2249. https://doi.org/10.1007/s00382-010-0931-y

Poveda G, Mesa óJ, Salazar LF et al (2005) The diurnal cycle of precipitation in the tropical Andes of Colombia. Mon Weather Rev 133(1):228–240. https://doi.org/10.1175/MWR-2853.1

Poveda G, Mesa Ó (1999) The low level westerly jet (Choco jet) and two other jets in Colombia: climatology and variability during ENSO phases. Rev Acad Colomb Cienc 23(89):517–528

Poveda G, Mesa ÓJ (2000) On the existence of Lloró (the rainiest locality on earth): enhanced ocean-land-atmosphere interaction by a low-level jet. Geophys Res Lett 27(11):1675–1678. https://doi.org/10.1029/1999GL006091

Poveda G, Waylen PR, Pulwarty RS (2006) Annual and inter-annual variability of the present climate in Northern South America and Southern Mesoamerica. Palaeogeography, Palaeoclimatology, Palaeoecology 234(1):3–27. https://doi.org/10.1016/j.palaeo.2005.10.031

Poveda G, Mesa Ó (1996) Las fases extremas del fenómeno ENSO (El Niño y la Niña) y su influencia sobre la hidrología de Colombia. Tecnología y Ciencias del Agua 11(1)

Riemann-Campe K, Fraedrich K, Lunkeit F (2009) Global climatology of convective available potential energy (CAPE) and convective inhibition (CIN) in ERA-40 reanalysis. Atmos Res 93(1):534–545. https://doi.org/10.1016/j.atmosres.2008.09.037

Rodell M, Beaudoing HK, L'Ecuyer TS et al (2015) The observed state of the water cycle in the early twenty-first century. J Clim 28(21):8289–8318. https://doi.org/10.1175/JCLI-D-14-00555.1

Rollings M, Merlis TM (2021) The observed relationship between Pacific SST variability and Hadley cell extent trends in reanalyses. J Clim 34(7):2511–2527. https://doi.org/10.1175/JCLI-D-20-0410.1

Ropelewski CF, Halpert MS (1987) Global and regional scale precipitation patterns associated with the El Niño/Southern Oscillation. Mon Weather Rev 115(8):1606–1626. https://doi.org/10.1175/1520-0493(1987)115<1606:GARSPP>2.0.CO;2

Ropelewski CF, Halpert MS (1989) Precipitation patterns associated with the high index phase of the Southern Oscillation. J Clim 2(3):268–284. https://doi.org/10.1175/1520-0442(1989)002<0268:PPAWTH>2.0.CO;2

Roy T, Martinez JA, Herrera-Estrada JE et al (2019) Role of moisture transport and recycling in characterizing droughts: perspectives from two recent U.S. droughts and the CFSv2 system. J Hydrometeorol 20(1):139–154. https://doi.org/10.1175/JHM-D-18-0159.1

Ruiz-Vásquez M, Arias PA, Martínez JA et al (2020) Effects of Amazon basin deforestation on regional atmospheric circulation and water vapor transport towards tropical South America. Clim Dyn 54(9):4169–4189. https://doi.org/10.1007/s00382-020-05223-4

Salas HD, Poveda G, Mesa óJ et al (2020) Generalized synchronization between ENSO and hydrological variables in Colombia: a recurrence quantification approach. Frontiers in Applied Mathematics and Statistics 6:3. https://doi.org/10.3389/fams.2020.00003

Sátori G, Williams E, Lemperger I (2009) Variability of global lightning activity on the ENSO time scale. Atmos Res 91(2):500–507. https://doi.org/10.1016/j.atmosres.2008.06.014

Serna L, Arias PA, Vieira S (2018) Las corrientes superficiales de chorro del Chocó y el Caribe durante los eventos de El Niño y El Niño Modoki. Revista de la Academia Colombiana de Ciencias Exactas, Físicas y Naturales 42(165):410–421. https://doi.org/10.18257/raccefyn.705

Shi P, Lu H, Leung LR, et al (2021) Significant land contributions to interannual predictability of East Asian summer monsoon rainfall. Earth's Future 9(2). https://doi.org/10.1029/2020EF001762

Shimizu MH, Ambrizzi T, Liebmann B (2017) Extreme precipitation events and their relationship with ENSO and MJO phases over northern South America. Int J Climatol 37(6):2977–2989. https://doi.org/10.1002/joc.4893

Sori R, Nieto R, Liberato M et al (2021) Oceanic versus terrestrial origin of El Niño Southern Oscillation-associated continental precipitation anomalies. Ann N Y Acad Sci 1:1–13. https://doi.org/10.1111/nyas.14665

Sulca J, Takahashi K, Espinoza JC et al (2018) Impacts of different ENSO flavors and tropical Pacific convection variability (ITCZ, SPCZ) on austral summer rainfall in South America, with a focus on Per. Int J Climatol 38(1):420–435. https://doi.org/10.1002/joc.5185

Todd A, Collins M, Lambert FH et al (2018) Diagnosing ENSO and global warming tropical precipitation shifts using surface relative humidity and temperature. J Clim 31(4):1413–1433. https://doi.org/10.1175/JCLI-D-17-0354.1

Verdin K, Verdin J (1999) A topological system for delineation and codification of the Earth's river basins. J Hydrol 218(1):1–12. https://doi.org/10.1016/S0022-1694(99)00011-6

Wang C (2004) ENSO, Atlantic climate variability, and the Walker and Hadley circulations, Springer Netherlands, pp 173–202. https://doi.org/10.1007/978-1-4020-2944-8_7

Yan Y, Wu H, Gu G et al (2020) Exploring the ENSO impact on basin-scale floods using hydrological simulations and TRMM precipitation. Geophys Res Lett 47(22):e2020GL089476. https://doi.org/10.1029/2020GL089476

Ye B, Genio ADD, Lo KKW (1998) CAPE variations in the current climate and in a climate change. J Clim 11(8):1997–2015. https://doi.org/10.1175/1520-0442(1998)011<1997:CVITHCC>2.0.CO;2

Zhang G, Wang Z (2013) Interannual variability of the Atlantic Hadley circulation in boreal summer and its impacts on tropical cyclone activity. J Clim 26(21):8529–8544. https://doi.org/10.1175/JCLI-D-12-00802.1

Publisher's Note Springer Nature remains neutral with regard to jurisdictional claims in published maps and institutional affiliations.